Supporting Information

Channel-Wall Functionalization in Covalent Organic Frameworks for the Enhancement of CO_2 Uptake and CO_2/N_2 Selectivity

Shang Zhao,‡[a,b] Bin Dong,‡[b] Rile Ge,[b] Chang Wang,[b] Xuedan Song,[c] Wei Ma,[a] Yu Wang,[b] Ce Hao,[c] Xinwen Guo,[c] and Yanan Gao*[b]

[a]Department of Chemistry, Dalian University of Technology, Dalian 116024, China

[b]Dalian Institute of Chemical Physics, Chinese Academy of Sciences, Dalian 116023, China

[c]State Key Laboratory of Fine Chemicals, Dalian University of Technology, Dalian 116024, China

‡S. Zhao and B. Dong contributed equally to this work.

*E-mail: ygao@dicp.ac.cn

Table S1 Elemental analysis results of $[HO]_{X\%}$-TAPH-COFs.

TAPH-COFs		C %	H %	N %
$[HO]_{25\%}$	Calcd	81.32	4.32	12.63
	Found	78.50	4.29	12.28
$[HO]_{50\%}$	Calcd	79.81	4.24	12.41
	Found	76.92	4.14	11.93
$[HO]_{75\%}$	Calcd	78.42	4.17	12.19
	Found	72.26	4.13	11.22
$[HO]_{100\%}$	Calcd	77.07	4.10	11.98
	Found	72.20	4.03	11.33

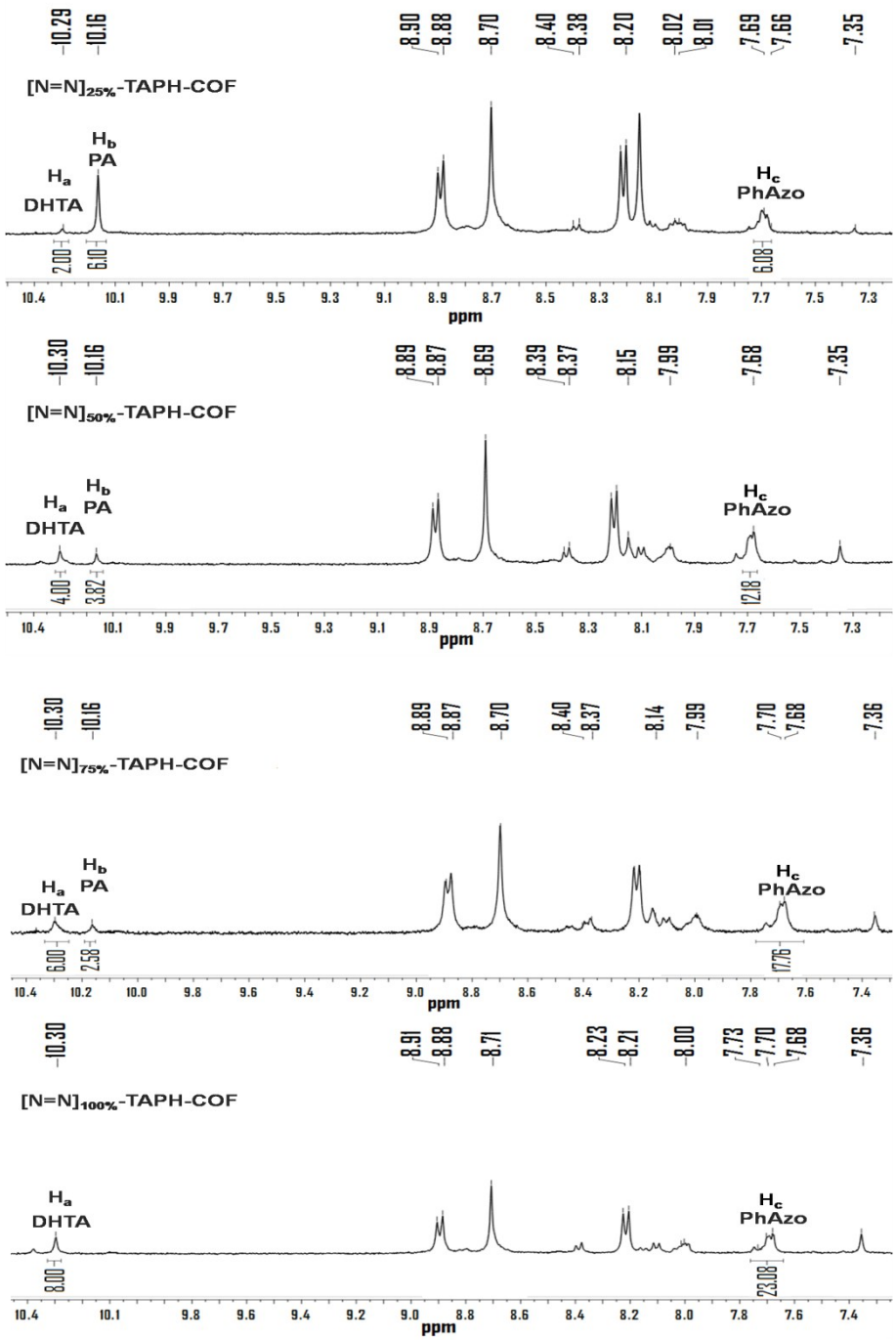

Fig. S1 ^{1}H NMR spectra of digested [N=N]$_{X\%}$-TAPH-COFs (X = 25, 50, 75, 100) in DMSO-d6 and DCl (6 M).

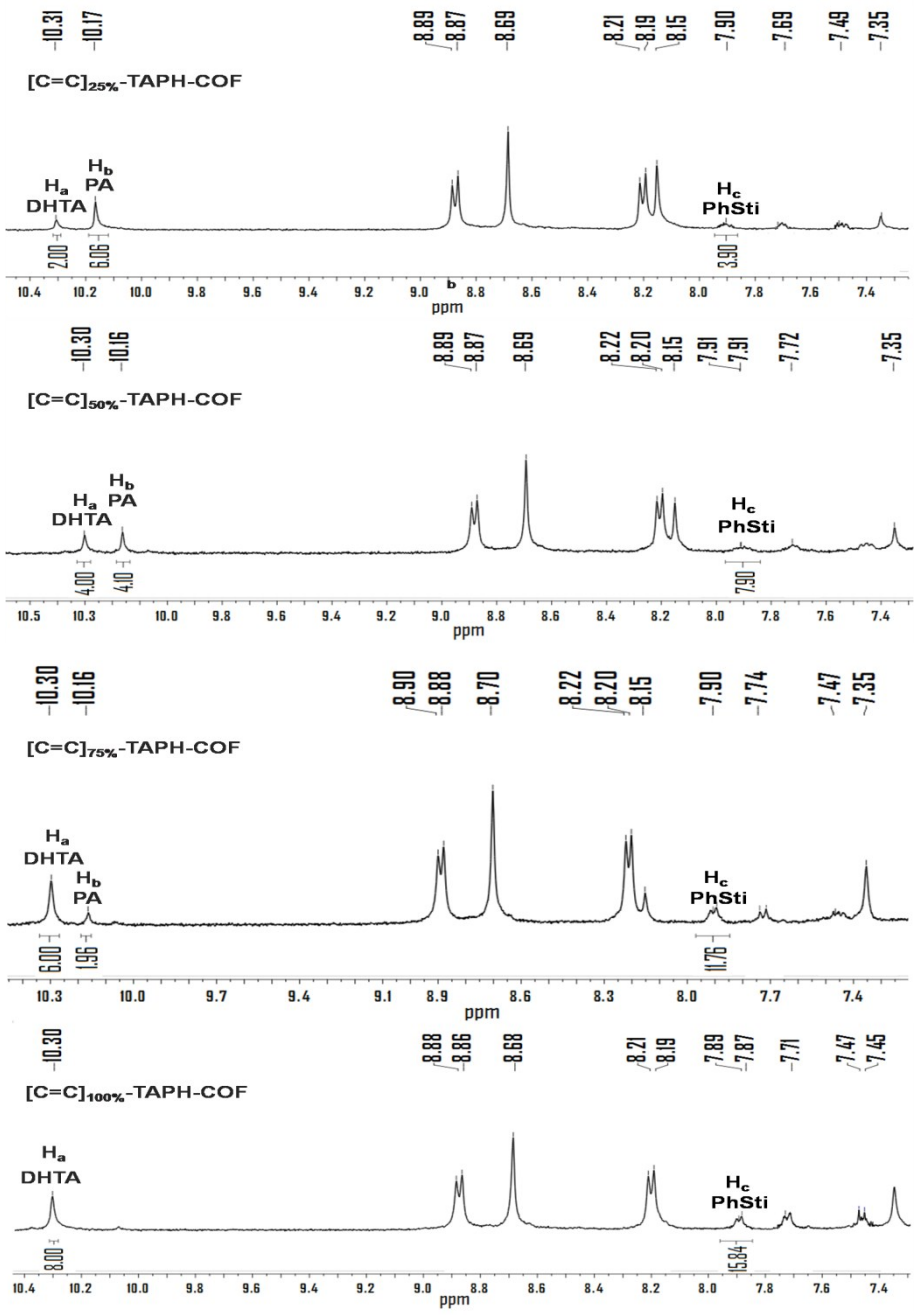

Fig. S2 ^{1}H NMR spectra of digested [C=C]$_{X\%}$-TAPH-COFs (X = 25, 50, 75, 100) in DMSO-d6 and DCl (6 M).

Table S2 Results of proton integration of digested $[N{=}N]_{X\%}$-TAPH-COFs.

	Fragment in solution	DHTA 10.30 ppm	PA 10.16 ppm	PhAzo 7.69 ppm
TAPH-COFs	Structures	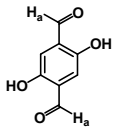	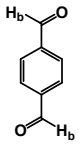	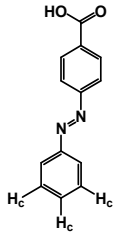
$[N{=}N]_{25\%}$	Proton integration	2.00	6.10	6.08
	Content of the azobenzene group	= 6.08/3(2.00+6.10) = 24.9%		
$[N{=}N]_{50\%}$	Proton integration	4.00	3.82	12.18
	Content of the azobenzene group	= 12.18/3(4.00+3.82) = 51.9%		
$[N{=}N]_{75\%}$	Proton integration	6.00	2.58	17.76
	Content of the azobenzene group	=17.76/3(6.00+2.58) = 69.0%		
$[N{=}N]_{100\%}$	Proton integration	8.00	0	23.08
	Content of the azobenzene group	= 23.08/3(8.00+0) = 96.2 %		

The content of the azobenzene group was calculated with the formula of $H_c/3(H_a+H_b)$. The calculated data were 24.9%, 51.9%, 69.0%, and 96.2%, which corresponded to the *X* values in $[N{=}N]_{25\%}$-TAPH-COF, $[N{=}N]_{50\%}$-TAPH-COF, $[N{=}N]_{75\%}$-TAPH-COF, and $[N{=}N]_{100\%}$-TAPH-COF, respectively.

Table S3 Results of proton integration of digested $[C{=}C]_{X\%}$-TAPH-COFs.

TAPH-COFs	Fragment in solution	DHTA 10.30 ppm	PA 10.16 ppm	PhSti 7.90 ppm
	Structures	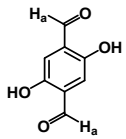	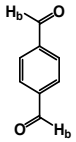	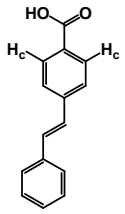
$[C{=}C]_{25\%}$	Proton integration	2.00	6.06	3.90
	Content of the stilbene group	= 3.90/2(2.00+6.06) = 24.2%		
$[C{=}C]_{50\%}$	Proton integration	4.00	4.10	7.90
	Content of the stilbene group	= 7.90/2(4.00+4.10) = 48.8%		
$[C{=}C]_{75\%}$	Proton integration	6.00	1.96	11.76
	Content of the stilbene group	= 11.76/2(6.00+1.96) = 73.9%		
$[C{=}C]_{100\%}$	Proton integration	8.00	0	15.84
	Content of the stilbene group	= 15.84/2(8.00+0) = 99.0%		

The content of the stilbene group was calculated with the formula of $H_c/2(H_a+H_b)$. The calculated data were 24.2%, 48.8%, 73.9%, and 99.0%, which corresponded to the *X* values in $[C{=}C]_{25\%}$-TAPH-COF, $[C{=}C]_{50\%}$-TAPH-COF, $[C{=}C]_{75\%}$-TAPH-COF, and $[C{=}C]_{100\%}$-TAPH-COF, respectively.

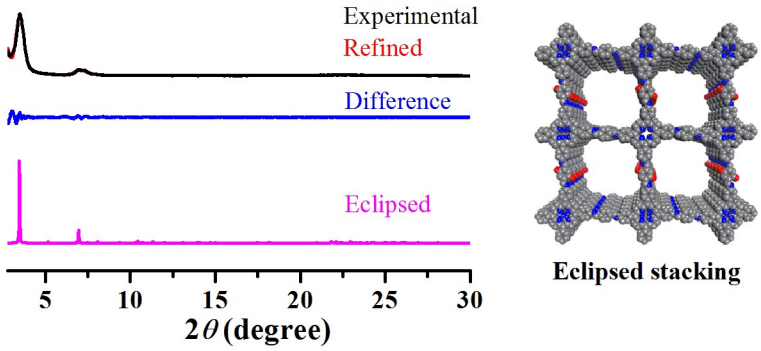

Fig. S3 PXRD patterns of $[HO]_{50\%}$-TAPH-COF: experimental (black), refined (red), the difference (blue, experimental minus refined profiles), and simulated patterns using eclipsed AA stacking mode (magenta). The unit cell was created with a *P2* space group of a = 35.3017 Å, b = 37.7221 Å, c = 3.8908 Å, and $\alpha = \beta = \gamma = 90°$.[S1] The use of lattice modeling and Pawley refinement processes led to an eclipsed AA stacking model that could reproduce the PXRD results in the peak position and intensity with R_{wp} of 4.9% and R_p of 3.9%.

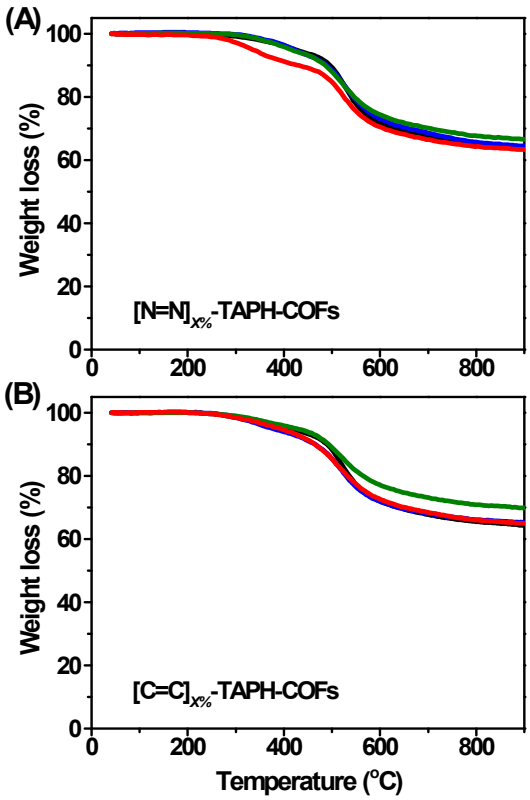

Fig. S4 TGA curves of (A) $[N{=}N]_{X\%}$-TAPH-COFs and (B) $[C{=}C]_{X\%}$-TAPH-COFs (X = 25: black, X = 50: blue, X = 75: olive, X = 100: red).

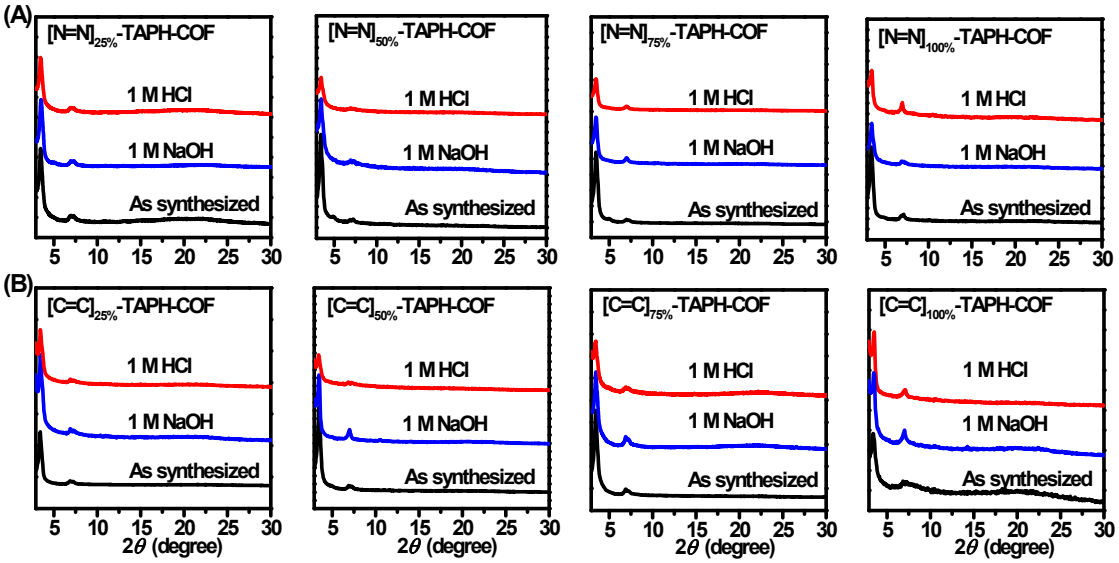

Fig. S5 PXRD patterns of (A) $[N{=}N]_{X\%}$-TAPH-COFs and (B) $[C{=}C]_{X\%}$-TAPH-COFs upon one-day treatment in 1 M HCl and 1 M NaOH at room temperature.

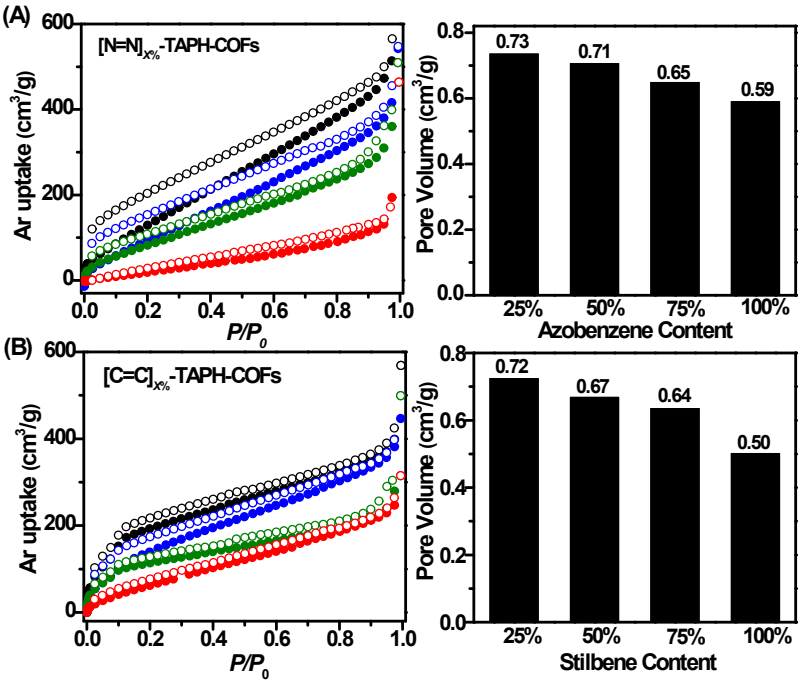

Fig. S6 Ar adsorption isotherm curves and pore volumes of (A) $[N{=}N]_{X\%}$-TAPH-COFs and (B) $[C{=}C]_{X\%}$-TAPH-COFs (X = 25: black, X = 50: blue, X = 75: olive, X = 100: red).

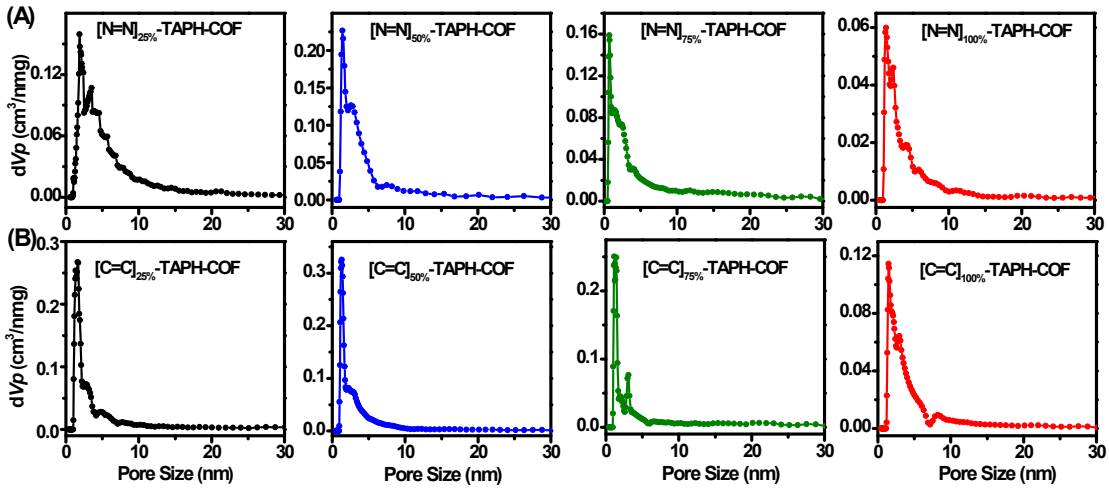

Fig. S7 Pore size distribution curves of (A) $[N{=}N]_{X\%}$-TAPH-COFs and (B) $[C{=}C]_{X\%}$-TAPH-COFs (X = 25, 50, 75, 100) by fitting NLDFT to the Ar adsorption data at 87 K. With the content of the functional groups increasing from 25% to 50%, 75%, and 100%, the pore size of $[N{=}N]_{X\%}$-TAPH-COFs decreased from 1.8 to 1.4, 1.2, and 1.0 nm, while the pore size of $[C{=}C]_{X\%}$-TAPH-COFs decreased from 1.6 to 1.3, 1.1, and 1.0 nm, respectively.

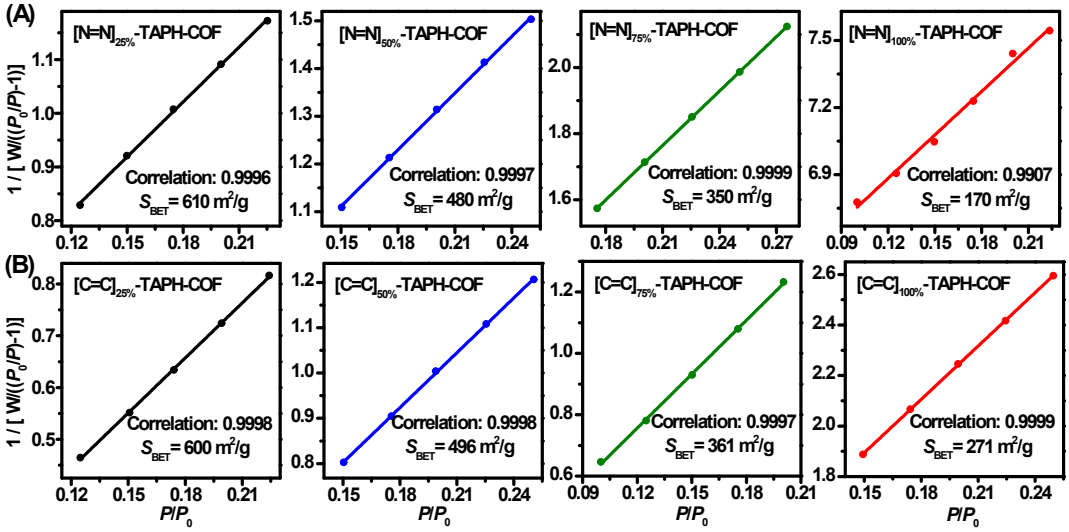

Fig. S8 BET surface area plots for $[N{=}N]_{X\%}$-TAPH-COFs and $[C{=}C]_{X\%}$-TAPH-COFs (X = 25, 50, 75, 100) calculated from the Ar adsorption isotherm at 87 K.

Table S4 Surface area, pore volume, and pore size of $[N{=}N]_{X\%}$-TAPH-COFs and $[C{=}C]_{X\%}$-TAPH-COFs calculated from the N_2 (77 K) and Ar (87 K) adsorptions.

TAPH-COFs	N_2 adsorption at 77 K			Ar adsorption at 87 K		
	S_{BET} (m^2/g)	Pore volume (cm^3/g)	Pore size (nm)	S_{BET} (m^2/g)	Pore volume (cm^3/g)	Pore size (nm)
$[N{=}N]_{25\%}$	702	0.72	1.7	610	0.73	1.8
$[N{=}N]_{50\%}$	560	0.64	1.4	480	0.71	1.4
$[N{=}N]_{75\%}$	320	0.59	1.3	350	0.65	1.2
$[N{=}N]_{100\%}$	250	0.54	1.2	170	0.59	1.0
$[C{=}C]_{25\%}$	680	0.70	1.7	600	0.72	1.6
$[C{=}C]_{50\%}$	460	0.66	1.6	496	0.67	1.3
$[C{=}C]_{75\%}$	390	0.55	1.3	361	0.64	1.1
$[C{=}C]_{100\%}$	310	0.51	1.2	271	0.50	1.0

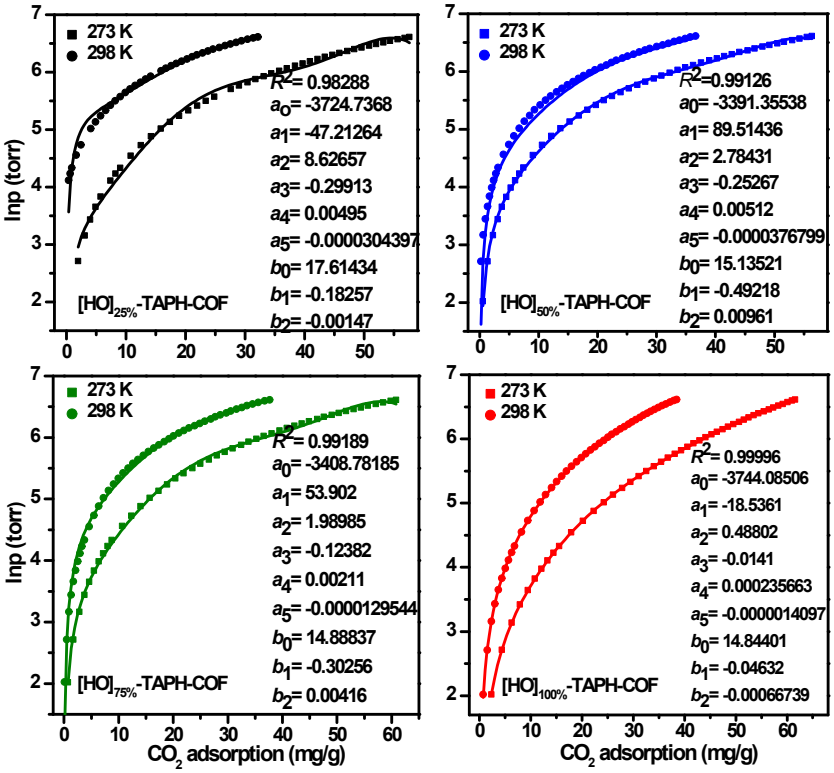

Fig. S9 The CO_2 adsorption isotherms (symbol) and the virial equation fits (line) for $[HO]_{X\%}$-TAPH-COFs (X = 25, 50, 75, 100) at 273 and 298 K, respectively.

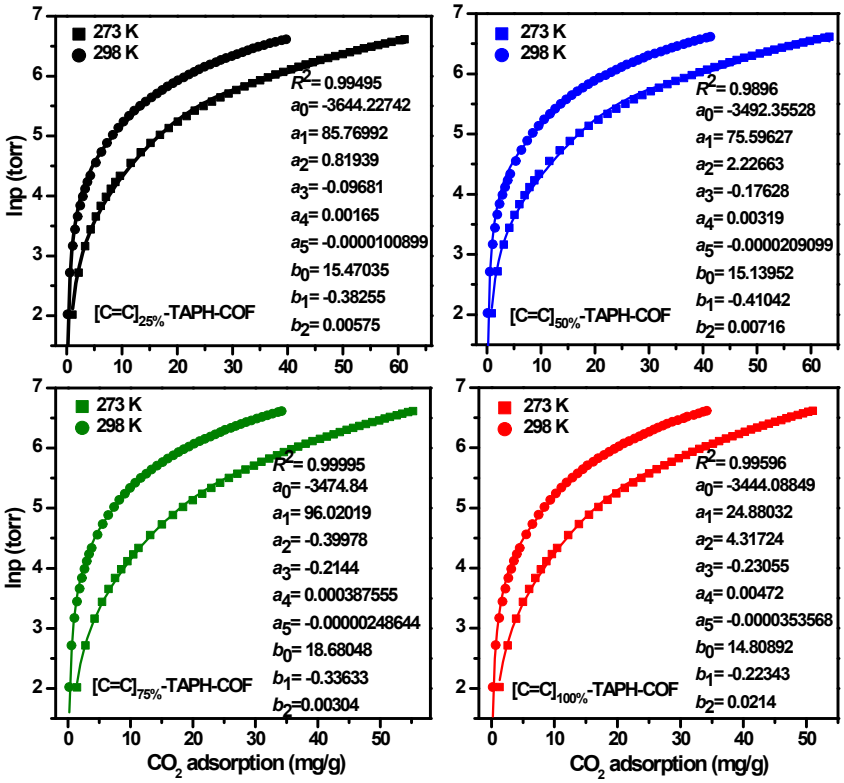

Fig. S10 The CO_2 adsorption isotherms (symbol) and the virial equation fits (line) for [C=C]$_{X\%}$-TAPH-COFs (X = 25, 50, 75, 100) at 273 and 298 K, respectively.

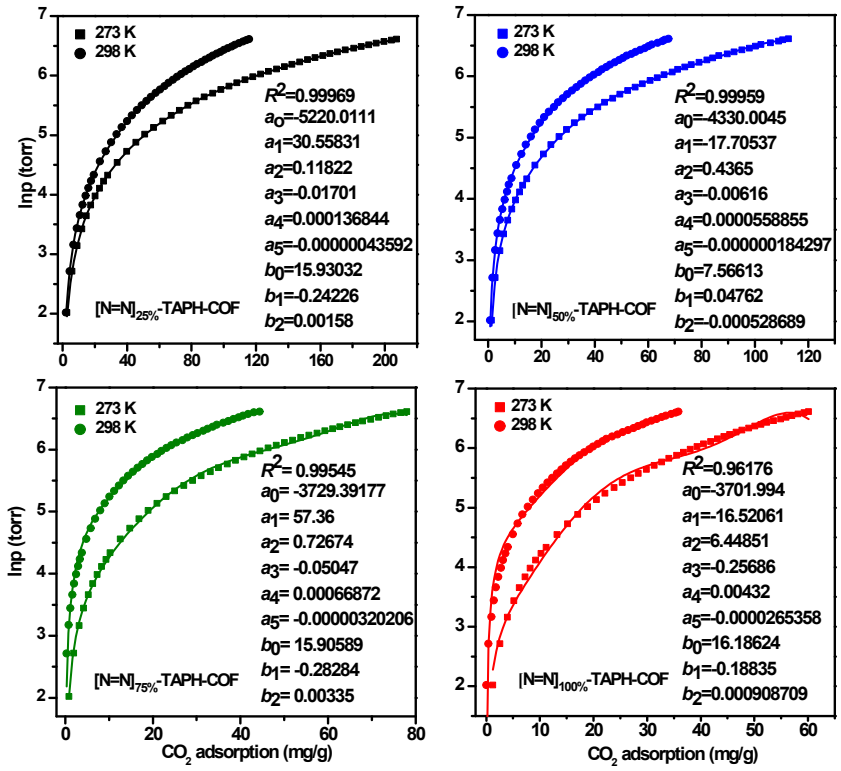

Fig. S11 The CO_2 adsorption isotherms (symbol) and the virial equation fits (line) for [N=N]$_{X\%}$-TAPH-COFs (X = 25, 50, 75, 100) at 273 and 298 K.

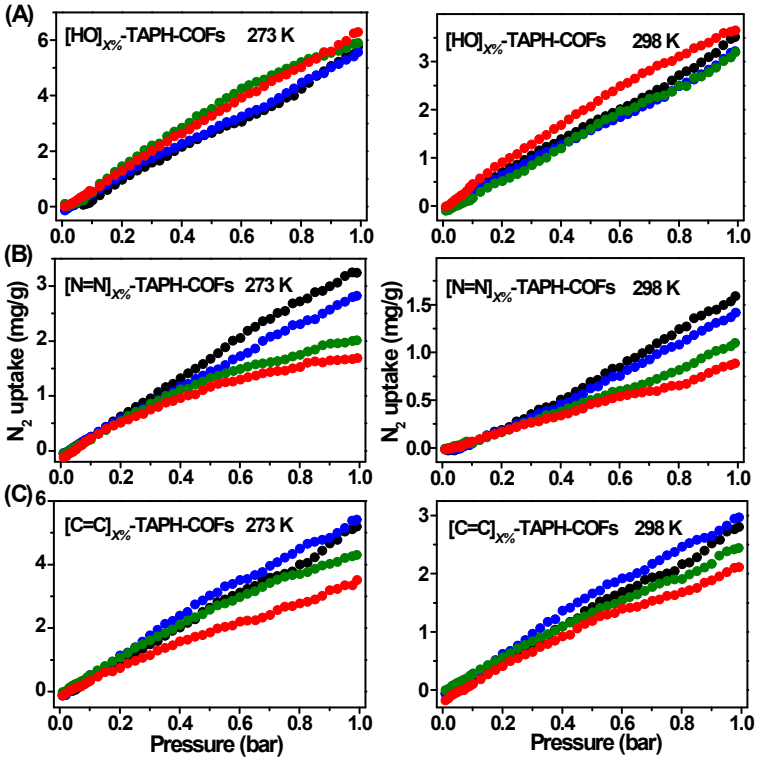

Fig. S12 N_2 adsorption isotherms measured at pressure of up to 1 bar at 273 K (left) and 298 K (right) of (A) $[HO]_{X\%}$-TAPH-COFs, (B) $[N{=}N]_{X\%}$-TAPH-COFs, and (C) $[C{=}C]_{X\%}$-TAPH-COFs with different contents of functional groups (X = 25: black, X = 50: blue, X = 75: olive, X = 100: red).

Table S5 CO_2 uptake (at 1 bar), N_2 uptake (at 1 bar), Q_{st} for CO_2, and CO_2/N_2 selectivity of $[HO]_{X\%}$-TAPH-COFs, $[N=N]_{X\%}$-TAPH-COFs, and $[C=C]_{X\%}$-TAPH-COFs.

TAPH-COFs	CO_2 uptake[a] (mg/g)	N_2 uptake[a] (mg/g)	Q_{st} for CO_2 (kJ/mol)	Selectivity[b]
				15/85 CO_2/N_2
$[HO]_{25\%}$	58 (32)	5.8 (3.5)	30.9	15 (9)
$[HO]_{50\%}$	56 (37)	5.6 (3.2)	28.2	13 (11)
$[HO]_{75\%}$	61 (38)	5.7 (3.2)	28.3	14 (12)
$[HO]_{100\%}$	62 (38)	6.3 (3.7)	31.1	16 (15)
$[N=N]_{25\%}$	207（115）	3.2 (1.6)	43.4	78 (111)
$[N=N]_{50\%}$	112 (67)	2.8 (1.4)	36.0	49 (59)
$[N=N]_{75\%}$	77 (44)	2.0 (1.1)	31.0	48 (53)
$[N=N]_{100\%}$	60 (39)	1.7 (0.9)	30.7	57 (74)
$[C=C]_{25\%}$	61 (40)	5.2 (2.8)	30.3	18 (16)
$[C=C]_{50\%}$	63 (41)	5.5 (3.0)	29.0	16 (14)
$[C=C]_{75\%}$	55 (34)	4.3 (2.4)	28.7	22 (16)
$[C=C]_{100\%}$	51 (34)	3.5 (2.2)	28.5	27 (22)

[a]Measured under 273 and 298 K (in parenthesis). [b]Calculated under 273 and 298 K (in parenthesis) using the IAST method.

Table S6 Summary of CO_2 uptake (at 1 bar), Q_{st} for CO_2, and CO_2/N_2 selectivity of the reported COFs.

COFs	CO_2 uptake[a] (mg/g)	Selectivity 15/85 CO_2/N_2	Q_{st} for CO_2 (kJ/mol)
COF-5[S2]	59	–	–
COF-103[S2]	76	–	–
TDCOF-5[S3]	92	–	21.8
ILCOF-1[S4]	60(32)	–	18.3
TH-COF-1[S5]	128	(19[b]/31[b])	31
COF-JLU2[S6]	217	77[c]	31
ATFG-COF[S7] (COF-JLU2)	173	(65[b]/151[c])	33.3
AB-COF (ACOF-1) [S7]	149	(88[b]/102[c])	29.7
ACOF-1[S8]	177	40[c]	27.6
TpPa-COF (MW)[S9]	218	32[c]	34.1
TAPB-TFPB[S10]	40	–	–
iPrTAPB-TFPB[S10]	31	–	–
TAPB-TFP[S10]	180	–	–
iPrTAPB-TFP[S10]	105	–	–
TAT-COF-2[S11]	77	5.9[b]	–
$[HO]_{100\%}$-H_2P-COF[S12]	63	(8[b])	36.4
$[HO_2C]_{100\%}$-H_2P-COF[S12]	174	(77[b])	43.5
$[AcOH]_{50}$-H_2P-COF[S13]	117	–	17.8
$[EtOH]_{50}$-H_2P-COF[S13]	124	–	19.7
$[EtNH_2]_{50}$-H_2P-COF[S13]	157	–	20.9
N-COF[S14]	120 (64)[d]	–	–

[a]Measured under 273 and 298 K (in parenthesis). [b]Calculated under 273 and 298 K (in parenthesis) using the IAST method. [c]Calculated under 273 and 298 K (in parenthesis) using the Henry method. [d]At 1 atm.

Reference

(S1) X. Chen, J. Gao, D. Jiang, *Chem. Lett.*, **2015**, *44*, 1257–1259.

(S2) H. Furukawa, O. M. Yaghi, *J. Am. Chem. Soc.*, **2009**, *131*, 8875–8883.

(S3) Z. Kahveci, T. Islamoglu, G. A. Shar, R. Ding, H. M. El-Kaderi, *CrystEngComm*, **2013**, *15*, 1524–1527.

(S4) M. G. Rabbani, A. K. Sekizkardes, Z. Kahveci, T. E. Reich, R. Ding, H. M. El-Kaderi, *Chem. Eur. J.*, **2013**, *19*, 3324–3328.

(S5) L. Wang, B. Dong, R. Ge, F. Jiang, J. Xiong, Y. Gao, J. Xu, *Micropor. Mesopor. Mat.*, **2016**, *224*, 95–99.

(S6) Z. Li, Y. Zhi, X. Feng, X. Ding, Y. Zou, X. Liu, Y. Mu, *Chem. Eur. J.*, **2015**, *21*, 12079–12084.

(S7) L. Stegbauer, M. W. Hahn, A. Jentys, G. Savasci, C. Ochsenfeld, J. A. Lercher, B. V. Lotsch, *Chem. Mater.*, **2015**, *27*, 7874–7881.

(S8) Z. Li, X. Feng, Y. Zou, Y. Zhang, H. Xia, X. Liu, Y. Mu, *Chem. Commun.*, **2014**, *50*, 13825–13828.

(S9) H. Wei, S. Chai, N. Hu, Z. Yang, L. Wei, L. Wang, *Chem. Commun.*, **2015**, *51*, 12178–12181.

(S10) D. Kaleeswaran, P. Vishnoi, R. Murugavel, *J. Mater. Chem. C*, **2015**, *3*, 7159–7171.

(S11) Y.-F. Xie, S.-Y. Ding, J.-M. Liu, W. Wang, Q.-Y. Zheng, *J. Mater. Chem. C*, **2015**, *3*, 10066–10069.

(S12) N. Huang, X. Chen, R. Krishna, D. Jiang, *Angew. Chem. Int. Ed.*, **2015**, *54*, 2986–2990.

(S13) N. Huang, R. Krishna, D. Jiang, *J. Am. Chem. Soc.*, **2015**, *137*, 7079–7082.

(S14) Q. Gao, L. Bai, X. Zhang, P. Wang, P. Li, Y. Zeng, R. Zou, Y. Zhao, *Chin. J. Chem.*, **2015**, *33*, 90–94.